PLOS ONE

RESEARCH ARTICLE

High-sensitivity calcium biosensor on the mitochondrial surface reveals that IP3R channels participate in the reticular Ca^{2+} leak towards mitochondria

Yves Gouriou[1,2☯*], **Fabrice Gonnot**[1,2☯], **Mariam Wehbi**[1,2], **Camille Brun**[1,2], **Ludovic Gomez**[1,2], **Gabriel Bidaux**[1,2*]

1 Univ-Lyon CarMeN Laboratory, Inserm U1060, Université Claude Bernard Lyon 1, INRAE, Bron, France, **2** Hospices Civils de Lyon, Groupement Hospitalier EST, Département de Cardiologie, IHU-OPERA Bâtiment B13, Bron, France

☯ These authors contributed equally to this work.
* yves.gouriou@univ-lyon1.fr (YG); gabriel.bidaux@inserm.fr (GB)

Citation: Gouriou Y, Gonnot F, Wehbi M, Brun C, Gomez L, Bidaux G (2023) High-sensitivity calcium biosensor on the mitochondrial surface reveals that IP3R channels participate in the reticular Ca^{2+} leak towards mitochondria. PLoS ONE 18(6): e0285670. https://doi.org/10.1371/journal.pone.0285670

Editor: Agustín Guerrero-Hernandez, Cinvestav-IPN, MEXICO

Received: January 4, 2023

Accepted: April 27, 2023

Published: June 9, 2023

Data Availability Statement: The datasets generated in this paper are available from figshare at: https://doi.org/10.6084/m9.figshare.22309429.v1.

Funding: G.B "Targeting Mitochondria to Treat Heart Disease: MitoCardia" (16 CVD 04) https://www.fondationleducq.org/ L.G "Cardiocare" (ANR n °16-CE17-0020-01) of the French National Research Agency (ANR) https://anr.fr/en/ The funders had no role in study design, data collection

Abstract

Genetically encoded biosensors based on fluorescent proteins (FPs) are widely used to monitor dynamics and sub-cellular spatial distribution of calcium ion (Ca^{2+}) fluxes and their role in intracellular signaling pathways. The development of different mutations in the Ca^{2+}-sensitive elements of the cameleon probes has allowed sensitive range of Ca^{2+} measurements in almost all cellular compartments. Region of the endoplasmic reticulum (ER) tethered to mitochondria, named as the mitochondrial-associated membranes (MAMs), has received an extended attention since the last 5 years. Indeed, as MAMs are essential for calcium homeostasis and mitochondrial function, molecular tools have been developed to assess quantitatively Ca^{2+} levels in the MAMs. However, sensitivity of the first generation Ca^{2+} biosensors on the surface of the outer-mitochondrial membrane (OMM) do not allow to measure μM or sub-μM changes in Ca^{2+} concentration which prevents to measure the native activity (unstimulated exogenously) of endogenous channels. In this study, we assembled a new ratiometric highly sensitive Ca^{2+} biosensor expressed on the surface of the outer-mitochondrial membrane (OMM). It allows the detection of smaller differences than the previous biosensor in or at proximity of the MAMs. Noteworthy, we demonstrated that IP3-receptors have an endogenous activity which participate to the Ca^{2+} leak channel on the surface of the OMM during hypoxia or when SERCA activity is blocked.

Introduction

Initially, the cytotoxic role of calcium ions (Ca^{2+}) in ischemia was published over 40 years ago [1, 2]. The Ca^{2+} overload results from an unbalance of cell homeostatic pathways regulating Ca^{2+} influx, efflux and release from internal stores. Release of Ca^{2+} from the endoplasmic reticulum (ER) has been suggested to be the initial signal for ER dysfunction in ischemia [3]. The alteration of Ca^{2+} ATPase pumps due to the lack of energy supply, uncovers the preexisting ER

and analysis, decision to publish, or preparation of the manuscript.

Competing interests: The authors have declared that no competing interests exist.

calcium leakage through different channels and receptors participating in the ischemia-induced Ca^{2+} overload [4]. In non-excitable cells, the main Ca^{2+} release channel is the inositol 1,4,5-trisphosphate receptor (IP3Rs). IP3R channels are key elements of Ca^{2+} signaling machinery and reside in close proximity to the interface between ER and mitochondria micro-domains to facilitate the transfer of Ca^{2+} ions [5–7]. In ischemic condition, the Ca^{2+}-sensing receptor (CaR) has been shown to be activated in different models of ischemia/reperfusion [8–10]. These receptors elicit phospholipase C-mediated inositol triphosphate (IP3) formation, leading to a cytosolic Ca^{2+} elevation. Yet it remains unclear if IP3Rs could participate in both ER Ca^{2+} leak and cytosolic Ca^{2+} overload, not only at the early phase of the reoxygenation [11] but also during the hypoxic period [12]. Thanks to the development of new biosensors this question can now be assessed by using targeted Ca^{2+}-sensitive fluorescent proteins.

The engineering of genetically encoded fluorescent biosensors, based on green fluorescent protein (GFP) has expanded the versatility of metabolites quantification in signaling pathway networks study. Since its discovery in the 1990s [13], GFP mutants have been extensively developed in a wide range of fluorescent proteins (FPs) with optimized brightness, photostability, folding and pH sensitivity. These optimizations of FPs have allowed the generation of robust tunable FRET-based biosensors to study Ca^{2+} signaling pathways. Indeed, the most common FRET biosensors are the Ca^{2+} sensitive cameleons based on CFP and YFP variants linked together by a Ca^{2+} binding domain from calmodulin and a calmodulin-binding domain from M13 skeletal-muscle myosin light-chain kinase [14]. Originally described in 2006 by Palmer et al., the Dcpv (cameleons) has been evolved into several variants: D1, D2, D3, D4 with different Ca^{2+} affinities and different cellular localization signals [14]. Cytosolic, mitochondrial and reticular cameleons Ca^{2+} biosensors have been generated and in 2010, Giacomello et al. have developed a GFP-based Ca^{2+} probe (N33D1cpv) localized on the outer mitochondrial membrane (OMM) suitable to monitor "Ca^{2+} hotspots" which means high Ca^{2+} levels from 1μM to 200–300μM [15] in a limited cellular area. The targeted sequence of the biosensor was based on the first 33 amino acids of TOM20 (N33), an endogenous protein of the OMM. Currently, there is no biosensor available to measure small variations of Ca^{2+} at the mitochondrial-associated membranes (MAMs) level.

In the present study, we assembled a new mitochondrial-surface GFP-based Ca^{2+} indicator derived from the GFP-based Ca^{2+} biosensor N33D1cpv, with a higher affinity for Ca^{2+} allowing sensitive Ca^{2+} measurements at the cytosolic surface of the OMM. By means of N33D3cpv biosensor, we showed that either genetic suppression or the pharmacological inhibition of endogenous IP3R activity reduced the speed of ER Ca^{2+} leak on the surface of the OMM during hypoxia.

Results and discussion

Generation of a new mitochondrial-surface targeted GFP-based Ca^{2+} indicator

First of all, we substituted the D1 Ca^{2+}-binding domain of N33D1cpv [15] by the D3 Ca^{2+}-binding domain of the cytosolic biosensor D3cpv, which has a higher Ca^{2+} affinity. This new Ca^{2+} indicator was called N33D3cpv (Fig 1A). The D3 ligand domain has a dissociation constant (Kd) of 0.6μM that is particularly adapted to the range of low intensity Ca^{2+} variations in the cytosol (range of Ca^{2+} changes from 0.1μM to 10μM). By means of confocal imaging analysis, we validated the N33D3cpv localization around the outer-mitochondrial membrane (OMM) as described for N33D1cpv indicator [15]. Cells transfected with N33D3cpv indicator together with a mitochondrial staining (mitotracker deep-red) showed a donut-like N33D3cpv fluorescence while mitotracker deep-red labelled the interior of mitochondria (Fig 1B, left

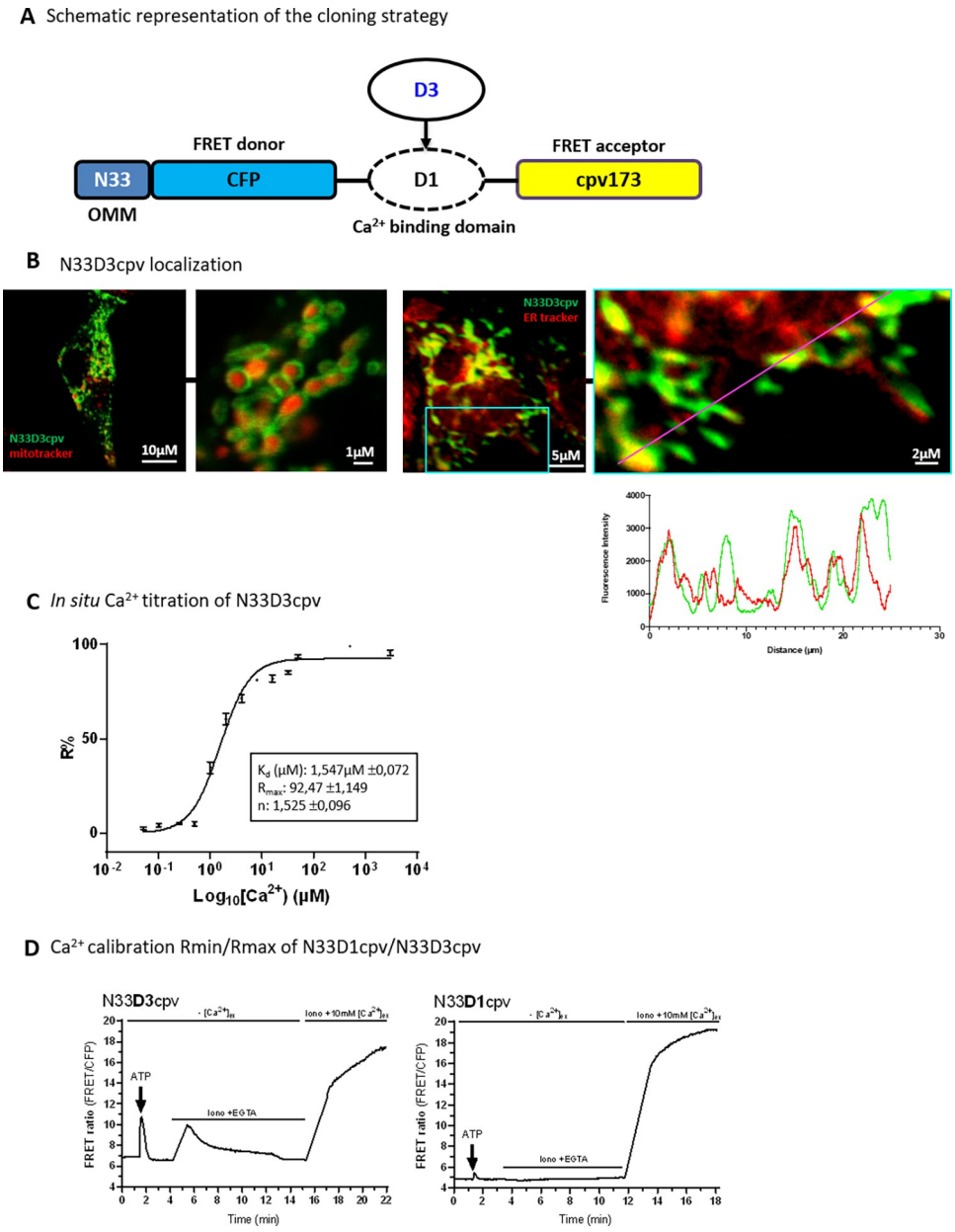

Fig 1. Characterization of N33D3cpv. (**A**) Schematic representation of the cloning strategy. Original Ca^{2+} biosensor N33D1cpv is composed of a signal addressing sequence (N33) coding for an outer mitochondrial membrane (OMM) peptide, the FRET donor (CFP: Cyan Fluorescent Protein), the Ca^{2+}-binding domain D1 and the FRET acceptor (cpv173: circularly permutated venus protein). N33D3cpv was generated by replacing D1 Ca^{2+}-binding domain with the D3 domain. (**B**) (left panel) Confocal images of H9c2 cell expressing N33D3cpv biosensor (green) and stained with a mitochondrial marker (mitotracker deep red). (right panel) Confocal images of H9c2 cell expressing N33D3cpv biosensor (green) and stained with an ER marker (ER tracker red). Line scan analysis of fluorescent intensity of green (N33D3cpv) and red fluorescence (ER tracker) (right panel). Zoomed-in panel for this analysis is represented on the original image by a blue square. (**C**) *In situ* Ca^{2+} titration assay of N33D3cpv with the fit values shown in the box. Data plotted: mean ± SEM ($n \geq 9$) cells for each [Ca^{2+}]. (**D**) Representative kinetics of FRET ratio (FRET/CFP) of H9C2 cells stimulated with 100µM ATP in Ca^{2+} free extracellular medium then permeabilized with ionomycin (5µM) in an intracellular medium containing EGTA (600µM) and BAPTA-AM (5µM) then finally perfused with an intracellular medium containing $CaCl_2$ (10mM). (Left panel) N33D3cpv. (Right panel) N33D1cpv. Raw values of FRET ratio are presented (FRET canal/CFP).

https://doi.org/10.1371/journal.pone.0285670.g001

panel). Colocalization study between N33D3cpv and ERtracker red revealed a partial colocalization in small spots which confirmed what have been observed in other models that only a part of the mitochondrial network is juxtaposed with the ER [16] (Fig 1B, right panel). Finally, we took advantage of the original protocol published by Palmer A. and Tsien R. [17], to perform an *in situ* calibration in order to compare with N33D1cpv the two key parameters, Ca^{2+} concentration and the dynamic range, for the N33D3cpv indicator (Fig 1C). We found a Kd of 1.5μM for N33D3cpv with the Ca^{2+} titration curve (Fig 1C) whereas N33D1cpv was reported having two Kd at: 18.61μM and 135.41μM [15]. We also measured for each set of experiments the dynamic range for each probe. Briefly, Ca^{2+}-buffered and Ca^{2+}-saturated solutions were applied on permeabilized H9c2 rat cardiomyoblast cells, and variation of $[Ca^{2+}]$ outside OMM ($[Ca^{2+}]_{OMM}$) was measured after IP3-mediated Ca^{2+} release by ATP stimulation (Fig 1D). We observed that the variation of FRET ratio, triggered by ATP stimulation, was 6-fold greater in N33D3cpv compared to the original N33D1cpv. This confirms the higher sensitivity of N33D3cpv indicator for physiological Ca^{2+} fluxes on the surface of the OMM.

Ca^{2+} affinity of the new generated N33D3cpv indicator

A higher affinity to Ca^{2+} would enable detection of a low Ca^{2+} amplitude and would also improve the temporal sensitivity required to study calcium dynamics. To confirm this point, we used three different Ca^{2+}-mobilizing stimuli and compared the responses measured by N33D1cpv and N33D3cpv indicators. We have chosen fast, slow and long-lasting kinetics of Ca^{2+} release on the surface of the OMM induced by ATP or oxygen glucose deprivation (OGD), respectively without external Ca^{2+}. We also used cyclopiazonic acid (CPA) to block SERCA pump activity in order to visualize the slow ER Ca^{2+} leakage. To compare both indicators' sensitivities and dynamics, we plotted them on the same graph by normalizing the FRET-ratio (F) with the baseline FRET-ratio value (F_0). At first, we compared the amplitude of the Ca^{2+} response following an ATP stimulus and we observed that the peak of averaged F/F_0 ratio was greater with N33D3cpv than with N33D1cpv: 1.573 and 1.107, respectively (Fig 2A). Second, we stimulated with CPA, a SERCA pump blocker that uncovers the slow passive Ca^{2+} leakage from the endoplasmic reticulum (ER). The peak of averaged F/F_0 ratio was greater with N33D3cpv than with N33D1cpv, 1.426 and 1.123 respectively and we observed also a difference in the decay of Ca^{2+} level (Fig 2B). Third, we performed an OGD to compare the indicators' responses and we observed that the peak of averaged F/F_0 ratio was once again greater with N33D3cpv than with N33D1cpv, 1.439 and 1.131 respectively (Fig 2C). As expected, due to its higher Kd for Ca^{2+} (Kds at 18.61μM and 135.41μM), N33D1cpv biosensor was not sensitive enough to efficiently discriminate the variations in $[Ca^{2+}]_{OMM}$ in these three conditions (Fig 2D). Indeed, after calibration, $[Ca^{2+}]_{OMM}$ estimated with N33D1cpv biosensor, in resting or stimulated (ATP, CPA or OGD) H9c2 rat cardiomyoblasts, showed a lot of negative values that reported a measure below the dynamic range of the biosensor (Fig 2D, ΔR% between 0,2–6). Conversely, N33D3cpv allowed us to perform accurate and reproducible measurements of $[Ca^{2+}]_{OMM}$ of 0.142±0.108 μM, 0.442±0.164 μM 0.426±0.082 μM, 0.434±0.051 μM, 0.2521 ±0.080 μM and 0.474±0.040 μM in basal, 50μM ATP, 100μM ATP, 5μM CPA, 20μM CPA and OGD conditions, respectively (S1G Fig and Fig 2E, ΔR% between 17–40). Altogether, these results clearly demonstrate the enhanced sensitivity of the new N33D3cpv sensor and its ability to detect lower variations in $[Ca^{2+}]_{OMM}$.

Physiological application of the newly generated N33D3cpv Ca^{2+} indicator

In ischemic condition, the lack of energy supply ceases Ca^{2+} ATPase pumps and depletes ER Ca^{2+} stores. Indeed, we previously demonstrated the rapid decrease of cytosolic and

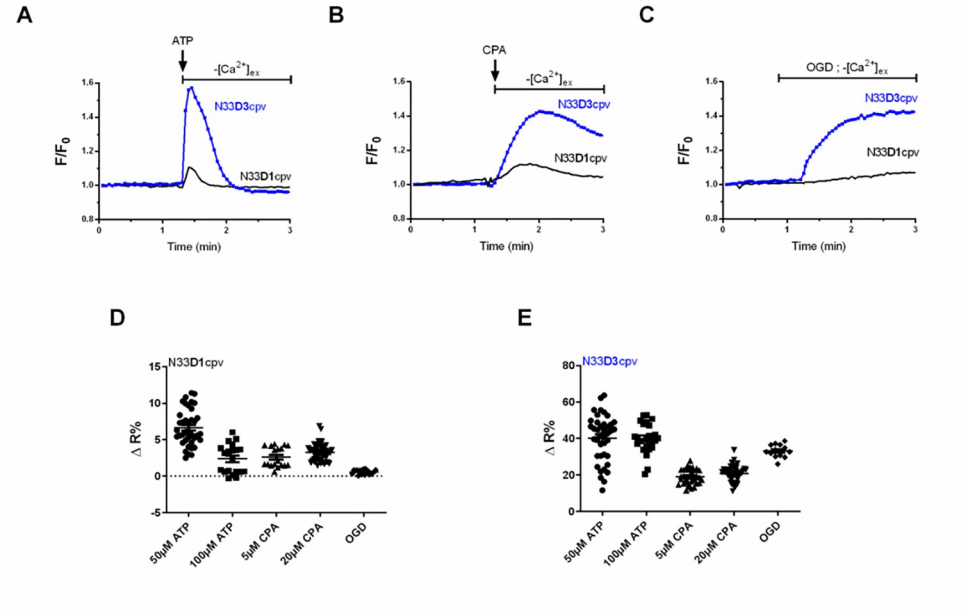

F

Mann-Whitney test	Significant	Adjusted P Value
50μM ATP N33D1cpv vs. 50μM ATP N33D3cpv	Yes	<0.0001
100μM ATP N33D1cpv vs. 100μM ATP N33D3cpv	Yes	<0.0001
5μM CPA N33D1cpv vs. 5μM CPA N33D3cpv	Yes	<0.0001
20μM CPA N33D1cpv vs. 20μM CPA N33D3cpv	Yes	<0.0001
OGD N33D1cpv vs. OGD N33D3cpv	Yes	<0.0001

Fig 2. Sensitivity of N33D1cpv and N33D3cpv biosensors in OMM. (**A**) Change in $[Ca^{2+}]_{OMM}$ induced by a 100 μM ATP stimulation, using either N33D1cpv (black) or N33D3cpv (blue) in absence of external Ca^{2+}. (**B**) Changes in $[Ca^{2+}]_{OMM}$ induced by 5 μM cyclopiazonic acid (CPA) stimulation, using N33D1cpv (black) or N33D3cpv (blue) in absence of external Ca^{2+}. (**C**) Changes in $[Ca^{2+}]_{OMM}$ occurring during an oxygen glucose deprivation (OGD), using N33D1cpv (black) or N33D3cpv (blue) in absence of external Ca^{2+}. (**A**-**C**) Representative average FRET-ratio (F) normalized with the baseline FRET-ratio value (F_0). (**D**-**E**) Dot plots represent the mean ±SEM of ΔR% of the 2 probes (N33D1cpv and N33D3cpv, respectively), where ΔR% is calculated as % of the steady-state value (R_1) and its maximum value (R_2) after drugs stimulation (ATP, CPA) or OGD. N = 3–4, Fig 2D n = 39, 20, 18, 48, 19 and Fig 2E n = 40, 25, 34, 45, 13 respectively. (**F**) Statistical comparison of the two biosensors for each stimulus with a Mann-Whitney test (Normality Kolmogorov-Smirnov test).

https://doi.org/10.1371/journal.pone.0285670.g002

mitochondrial ATP levels upon ischemia. This decrease was concomitant with a rapid release of Ca^{2+} in the cytosol and in the mitochondria [18, 19]. Nevertheless, this mechanism of ER Ca^{2+} depletion remains unclear. Despite the fact that IP3Rs are the major release Ca^{2+} channels in non-excitable cells, their contribution during the ischemic period has not been assessed. We used a model of types-I/II/III IP3Rs triple knock-out (TKO) [20] to study their contribution in hypoxia-induced Ca^{2+} leak by using our new N33D3cpv indicator.

First, we controlled the TKO IP3Rs HeLa cells model. Immunoblotting against IP3R1, IP3R3 isoforms allowed us to show that, unlike the WT samples, no band at the expected size of about 314kDa was detected in the TKO samples (S1A–S1C Fig). We were not able to detect IP3R2 isoform in WT Hela cells (goat sc7278). A functional assay was done through the measurement of the Ca^{2+} levels using N33D3cpv indicator on stimulated HeLa cells with ATP. We observed an IP3-mediated Ca^{2+} release in WT cells and no response in TKO cells (S1D Fig). We thus confirmed the absence of IP3Rs activity in this model of TKO HeLa cells.

With the objective to assess the implication of IP3Rs in ER Ca^{2+} leak, we assessed the native activity of IP3R while blocking SERCA activity with CPA. We compared the Ca^{2+} responses

induced by CPA in WT and TKO HeLa cells with D3cpv (Fig 3A) and N33D3cpv indicators (Fig 3B). As reported in Fig 3, D3cpv was unable to detect any difference in the cytosol whereas N33D3cpv biosensor detected a significant decrease in the slope of Ca^{2+} accumulation around mitochondria in TKO IP3Rs (0.101±0.038) as compared to WT HeLa cells (0.154±0.052). Although these results may seem paradoxical, they are in the same line of evidence with prior studies which could not report difference in $[Ca^{2+}]_{cyto}$ after blockage of SERCA pumps in TKO and WT cells; whatever the biosensor used: Fura-2 (Kd 0.220μM) [20], GEM-GECO (Kd 0.340μM) [21]. These prior publications mostly supported the fact that TKO had no change in their ER Ca^{2+} stores. Interestingly, by means of GEM-CEPIA1er (Kd 558μM) or R-CEPIA1er (Kd 565μM) [21], Yue et al. reported a small decrease in the rate of ER Ca^{2+} release, what could be explained by the decrease in ER Ca^{2+} leak, that we observed on the surface of the OMM (Fig 3C). IP3R1 has been previously reported to exert an endogenous activity as leak channel in non-stimulated cells [22, 23]. The Ca^{2+} decrease that we observed on the surface of the OMM could thus be related to the loss of native IP3R activity or an increased Ca^{2+} removal by pumps or transporters (so as MCU in mitochondria). The latter hypothesis is very unlikely since SERCA pumps are inhibited by CPA in our experiments. In addition, Yue et al. additionally reported a decrease in SERCA-mediated Ca^{2+} uptake in TKO cells that would have been expected to enhance Ca^{2+} accumulation on the surface of the OMM. Finally, the increase in MAMs width, previously reported in the TKO cells [24], is expected to decrease MCU-mediated Ca^{2+} uptake in mitochondria, that would have also led to an increase in Ca^{2+} accumulation on the surface of the OMM. Altogether these results rather validate the hypothesis that endogenous IP3R activity participates in the ER Ca^{2+} leak when SERCA activity is pharmacologically inhibited.

We thus wondered whether the native activity of IP3Rs contributed to the ER Ca^{2+} leak during hypoxia. When Hela cells were incubated under oxygen glucose deprivation (OGD), an ER Ca^{2+} leak occurred which could be measured indirectly through the sustained Ca^{2+} increase both in the cytosol, $[Ca^{2+}]_{cyto}$ (Fig 3D) and in OMM surface, $[Ca^{2+}]_{OMM}$ (Fig 3E). In the S1E and S1F Fig, we reported that the precision of the measurements of steady-state $[Ca^{2+}]$ by D3cpv (SD: 0.097 and 0.102 for WT and TKO; S1E Fig) was 2-fold below the one of N33D3cpv (SD: 0.053 and 0.055 for WT and TKO; S1F Fig). Consequently, N33D3cpv could detect a smaller variation in $[Ca^{2+}]$ in WT than in TKO HeLa cells, at 0.098 ±0.064 μM and 0.120 ±0.068 μM, respectively (S1F Fig). We then analyzed the slope of the rise in $[Ca^{2+}]_{cyto}$ and in $[Ca^{2+}]_{OMM}$ and we found a significantly slower Ca^{2+} increase rate in TKO compared to WT HeLa cells both in the cytosol and on the OMM (Fig 3F). Interestingly, we detected a faster Ca^{2+} increase at the OMM level compared to the cytosol in WT cells but no difference in TKO cells. This result suggests a greater activity of IP3R on the surface of the OMM than in the whole ER membrane [24]. However, IP3R clusters participate as physical tethers in MAMs and the loss of IP3Rs has been reported to decrease the frequency of tight contact sites (10-50nm) in MAMs of TKO cells. This modification in MAMs structure could in turn delay the rise of Ca^{2+} on the surface of the OMM. In order to determine to which extent (i) the loss of IP3Rs activity and (ii) the modification in ER-mitochondrial contacts were involved in the observed decrease in the rate of Ca^{2+} accumulation on the surface of the OMMs during the hypoxia, we incubated WT Hela cells with U73122 to inhibit phospholipase C (PLC), which has a crucial role in the initiation of the activation of IP3Rs [25]. WT Hela cells were incubated with 10 μM U73122 (Fig 3G and 3H) and we detected a reduced rate of Ca^{2+} increase in the cytosol and in OMM surface in WT+ PLC inhibitor compared to WT HeLa (Fig 3I). Interestingly, it has been shown that the inhibition of PLC by U73122 was suppressing IP3R clustering induced by IP3-generating agonists or calcium ionophore [26]. This may explain the differences in calcium kinetics observed between the IP3R KO and the PLC inhibitor condition

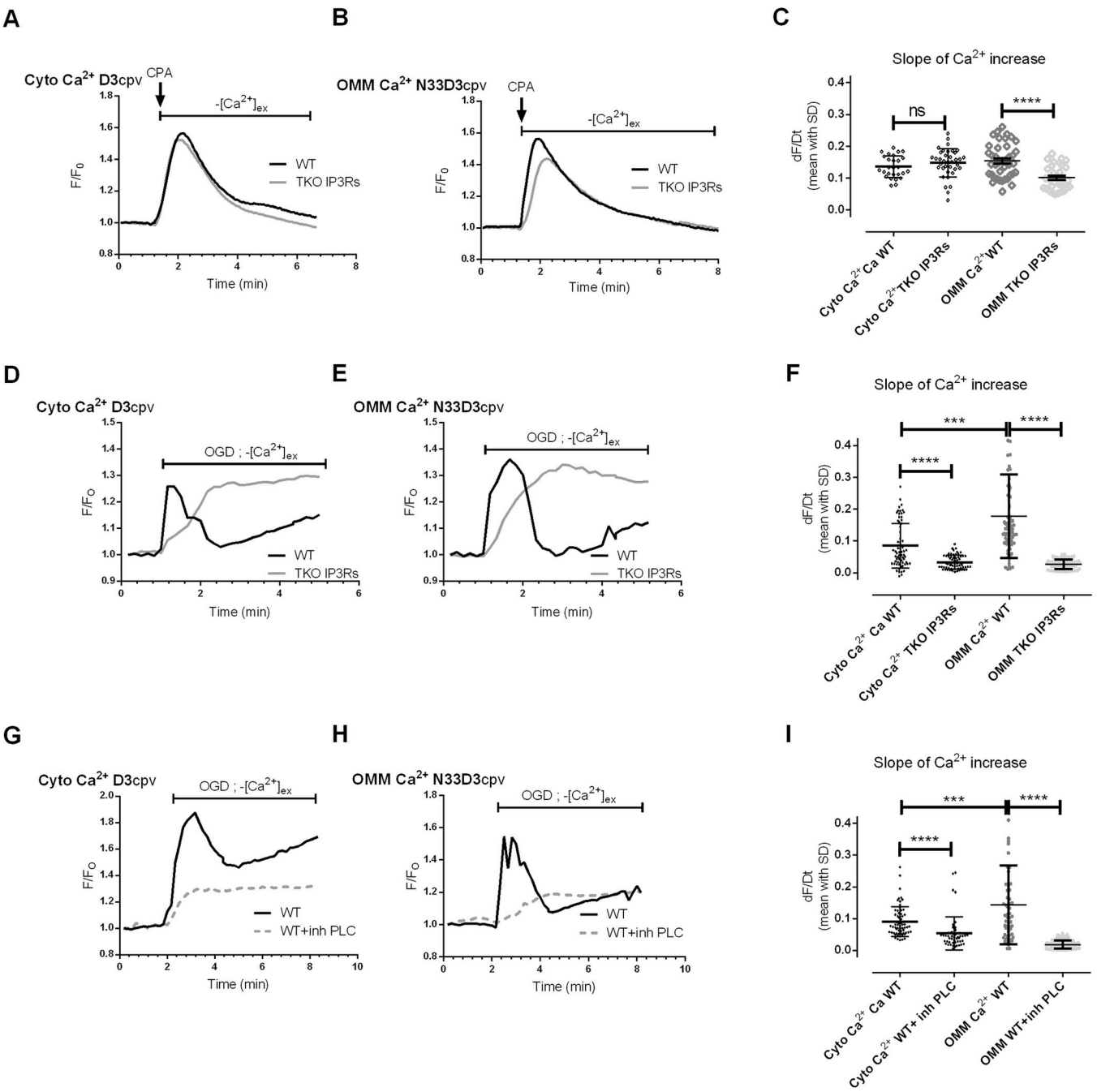

Fig 3. N33D3cpv Ca^{2+} biosensor study the role of IP3R channels in the passive ER Ca2+ leak. Time trace shows $[Ca^{2+}]_{cyto}$ (**A**) or $[Ca^{2+}]_{OMM}$ (**B**) measured with D3cpv and N33D3cpv, respectively, in absence of external Ca^{2+}, in WT (black) and TKO IP3Rs (grey) HeLa cells. A 5 μM cyclopiazonic acid (CPA) stimulation was applied to block SERCA activity in order to reveal the ER Ca^{2+} leak. Representative average FRET-ratio (F) normalized with the baseline FRET-ratio value (F_0). (C) Slope of the Ca^{2+} increase induced by cyclopiazonic acid (CPA) stimulation in WT and TKO IP3Rs HeLa cells N = 3–4 n = 27, 37, 42, 32 respectively. The normality of the samples was evaluated (Kolmogorov-Smirnov test), then an ordinary one-way ANOVA test with Holm-Šídák multiple comparisons test was performed to determine significance. Time trace shows $[Ca^{2+}]_{cyto}$ (**D**) or $[Ca^{2+}]_{OMM}$ (**E**) measured with D3cpv and N33D3cpv, respectively, in absence of external Ca^{2+}, in WT (black) and TKO IP3Rs (grey) HeLa cells. These cells were subjected to an oxygen glucose deprivation (OGD). Representative average FRET-ratio (F) normalized with the baseline FRET-ratio value (F_0). (**F**) Slope of the Ca^{2+} increase induced by OGD in WT and TKO IP3Rs HeLa cells. N = 3 n = 67, 64, 75, 83, respectively. Time trace shows $[Ca^{2+}]_{cyto}$ (**G**) or $[Ca^{2+}]_{OMM}$ (**H**) measured with D3cpv and N33D3cpv, respectively, in absence of external Ca^{2+}, in WT (black) and TKO IP3Rs (grey) HeLa cells. HeLa cells expressing D3cpv or N33D3cpv were treated with 10μM U73122 during an oxygen glucose deprivation (OGD). (**I**) Slope of the Ca^{2+} increase induced by OGD in WT HeLa cells with or without PLC inhibitor (10μM U73122). N = 3 n = 65, 50, 57, 84, respectively. Representative average FRET-ratio (F) normalized with the baseline FRET-ratio value (F_0). For non-normal distribution (Fig 3F–3I), an ANOVA kruskal-Wallis test with Dunn's multiple comparisons test was performed to determine significance. (**C, F, I**) Data shown represent the mean with standard deviation (SD) of at least 3–4 independent experiments (ns $p \geq 0.05$, * $p < 0.05$, ** $p < 0.01$, *** $p < 0.001$, **** $p < 0.0001$).

https://doi.org/10.1371/journal.pone.0285670.g003

(Fig 3D, 3E, 3G and 3H). Another interesting feature is the multiphasic calcium response that occurs upon OGD that is partially blunted in IP3R TKO cells. Others calcium cycling organelles have been showed to release calcium upon agonist-dependent IP3 generation such as the lysosomes and the golgi apparatus [27–29]. These others calcium stocks may also contribute to this complex calcium response during OGD. Altogether, these results confirmed that an endogenous IP3R activity participated in the passive ER Ca^{2+} leak occurring during hypoxia and was more specifically localized in the MAMs.

In conclusion, thanks to our newly designed D3cpv biosensor addressed to OMM, we showed that the endogenous IP3R activity participates in ER Ca^{2+} leak during hypoxia. This N33D3cpv biosensor allows very sensitive Ca^{2+} measurement on the surface of mitochondria and will help further researches in the field of ER-mitochondria homeostasis.

Material and methods

N33D3cpv construct strategy

A 1998 bp BamHI-XhoI fragment encompassing D3cpv was prepared from pcDNA-D3cpv, gifted from Roger Tsien (Addgene plasmid # 36323) [14], and subcloned between BamHI and XhoI restriction sites in pcDNA-N33D1cpv, gifted from Tullio Pozzan [15], to generate pcDNA-N33D3cpv (7583 bp). Created plasmid DNA sequence was confirmed by Sanger sequencing.

Cell culture and transfection

Rat cardiomyoblasts H9c2 (ATCC, CRL-1446) and WT / TKO -HeLa cells (kindly provided by Katsuhiko Mikoshiba at SIAIS, ShanghaiTech University, Shanghai, China) were routinely cultured in Dulbecco's Modified Eagle Medium (Gibco) supplemented with 10% fetal calf serum (PAN-biotech), 100 U/mL penicillin (Gibco), 100 μg/mL streptomycin (Gibco), 2 mM L-glutamine (Gibco) and incubated at 37˚C in 5% CO_2 in a damp atmosphere. Cells were regularly passaged by single-cell dissociation with 0.05% trypsin-EDTA (Gibco). For generation of transient transfectants, all DNAs (N33D1cpv and N33D3cpv) were transfected into cells using DharmaFECT Duo (Dharmacon, T-2010-03) according to manufacturer's instructions. Cells were plated on glass coverslips 24 hours before transfection and experiments were performed 48 hours after.

Immunoblotting

For Western-blotting, cell lysates were obtained by treating the cell monolayer with RIPA buffer complemented with protease and phosphatase inhibitors. Protein lysates were then cleared by centrifugation (17'000g for 20min). Total protein concentration was determined using bicinchoninic acid protein assay (Interchim, UP40840) and 25μg of denatured and reduced proteins of each sample was loaded on a 6% SDS-PAGE. For the IP3R1 immunoblotting (1/500, Abcam, ab5804) (S1B Fig), a 10% SDS-PAGE gel was used and the protein transfer was performed at low intensity overnight in a cold room. For the IP3R3 immunoblotting (1/1000, BD Biosciences, 610312) (S1C Fig), a 10% SDS-PAGE gel was used and the protein transfer was performed at low intensity overnight in a cold room.

After SDS-PAGE migration and electroblotting on polyvinylidene fluoride, the membranes were blocked with 5% non-fat milk and then incubated with the specific primary antibodies [rabbit anti-IP3R1 (Santa-Cruz, sc-28614; 1/500) and rabbit anti-TUBULIN (Santa-Cruz, sc-5286; 1/500)] (S1A Fig).

Blots were incubated with horseradish peroxidase (HRP)-coupled sheep anti-mouse IgG (GE Healthcare, NA931VS; 1/10000) and (HRP)-coupled goat anti-rabbit IgG (GE Healthcare, NA934VS; 1/10000), and developed with Clarity Western ECL Substrate (BioRad, 1705060). The band intensity was determined using Image Lab software (Bio-Rad).

Wide-field imaging

Living cells were imaged on an inverted epifluorescence microscope Leica DMi6000B using a 40x oil-immersion objective, with Lambda DG4 wavelength-switch xenon light source (Sutter Instruments), equipped with an ORCA-Flash4.0 digital CMOS camera C11440 (Hamamatsu). Pictures have been acquired with 200 ms acquisition time per frame, 10% fluorescence intensity manager (FIM) and an interval of 1 second for time-lapse. Cameleon fluorescent proteins were excited at a wavelength of 430nm and emissions were collected at 480nm and 530nm. Fluorescence ratio imaging was analysed using MetaFluor software (Molecular Devices). Experiments were carried out in controlled environment at 37˚C and cells were placed in Ca^{2+}-free buffer containing 140mM NaCl, 5mM KCl, 1mM $MgCl_2$, 10mM HEPES and 10 mM Glucose, adjusted to pH 7.4, supplemented with 1 mM EGTA.

Dynamic range method: In H9C2 cells expressing N33D3cpv or N33D1cpv, Rmin and Rmax were obtained upon permeabilization of the cells with 5μM ionomycin and a Ca^{2+}-free buffer containing 140mM NaCl, 5mM KCl, 1mM $MgCl_2$, 10mM HEPES and 10 mM Glucose, adjusted to pH 7.4, supplemented with 600μM EGTA. The Rmin was achieved by perfusing the cells with this medium containing 600μM EGTA and 5μM BAPTA-AM. The Rmax was achieved by perfusing the cells with a Ca^{2+} buffer containing 140mM NaCl, 5mM KCl, 1mM $MgCl_2$, 10mM HEPES and 10 mM Glucose, adjusted to pH 7.4, supplemented with 10mM CaCl2. R% is calculated as $R\% = (R - R_{min})/(R_{max} - R_{min}) \times 100$.

In situ Ca^{2+} titration assay: H9C2 cells expressing N33D3cpv were permeabilized with 100μM digitonin in a Ca^{2+}-free medium containing 600μM EGTA for 60 sec and then washed 3 times with the same medium without digitonin. Cells were then perfused with Ca^{2+} buffer containing 140mM NaCl, 5mM KCl, 1mM $MgCl_2$, 10mM HEPES and 10 mM Glucose, adjusted to pH 7.4, and known Ca^{2+} concentrations. At the end of each experiment, a saturating Ca^{2+} concentration (10mM) was applied. For $[Ca^{2+}]$ lower than 0,5μM, the buffer was supplied with BAPTA free acid and Ca^{2+}. The free $[Ca^{2+}]$ was estimated using MaxChelator. The results obtained were plotted as $\log_{10}[Ca^{2+}]$ (x-axis) and R% (y-axis) and fitted using Prism 9.0 (GraphPad) with the following equation: $y = (Rmax1 \times x^{n1})/(kd1^{n1} + x^{n1}) + (Rmax2 \times x^{n2})/(kd2^{n2} + x^{n2})$.

Oxygen-Glucose Deprivation (OGD) experiments

Cells were washed twice, placed in Ca^{2+}-containing buffer having 140mM NaCl, 5mM KCl, 1mM $MgCl_2$, 10 mM HEPES and 2mM $Na_2S_2O_4$, adjusted to pH 7.4, supplemented with 2mM $CaCl_2$. Cells were placed in a specifically manufactured bio-incubator (NewBrunswik, Galaxy 48R) connected with a 100% N_2 bottle. Oxygen level and temperature were monitored at 0.5% and at 37˚C respectively. An Okolab system with a specific hypoxic chamber was used to control the environmental constants (temperature, humidity and oxygen levels).

Confocal imaging

Living cells were imaged on an inverted confocal microscope Nikon A1R+ system using 40x oil-immersion objective with Argon laser (488-514nm) for the Cameleon excitation, Diode (642nm) for the Mitotracker Deep Red and diode (560nm) for the ERtracker Red. The images were acquired on living cells plated on glass coverslips.

Statistical analysis

Data processing and statistical analyses were conducted with Prism 9.0 (GraphPad) software. Before proceeding to any analysis, the normality of the samples was evaluated (Kolmogorov-Smirnov test). Unpaired *t*-test (for normal distribution) or Mann–Whitney test (for non-normal distribution) was used unless stated otherwise in the figure legends. *p*-values are indicated in figures. Data show mean with standard deviations (SD) calculated from at least three independent experiments. For single-cell imaging analysis, statistics were performed on n = number of cells to assess single-cell effect as well as heterogeneity between them. Both N and n values are indicated in the figure legends. A p value < 0.05 was considered significant.

Supporting information

S1 Fig. N33D3cpv Ca^{2+} biosensor to study the role of IP3R channels in the passive ER Ca2 + leak. (A) Immunoblotting against IP3R1 isoform (IP3R-I Santa-Cruz sc-28614) and tubulin in WT and TKO IP3Rs HeLa cells. Data shown represent the mean with standard deviation (SD) of 3 independent experiments, (* $p<0.05$). (B) Immunoblotting against IP3R1 receptor (Anti-IP3 receptor antibody Abcam ab5804) in WT and TKO IP3Rs Hela cells. Proteins normalized by using 2,2,2-Trichloroethanol (TCE) to visualize total protein content. Data shown represent the mean with standard deviation (SD) of 3 independent experiments, (* $p<0.05$). (C) Immunoblotting against IP3R3 receptor (IP3R3 BD 610312, 1/1000, MOUSE) in WT and TKO IP3Rs Hela cells. Proteins normalized by using 2,2,2-Trichloroethanol (TCE) to visualize total protein content. (D) $[Ca^{2+}]_{OMM}$ was estimated using N33D3cpv biosensor in WT and TKO IP3Rs HeLa cells treated with 100 μM Na, in absence of external Ca^{2+}. Representative average FRET-ratio (F) normalized with the baseline FRET-ratio value (F_0). (E) Steady-state $[Ca^{2+}]_{cyto}$ in WT and TKO IP3Rs HeLa cells. (F) Steady-state $[Ca^{2+}]_{OMM}$ in WT and TKO IP3Rs HeLa cells. The normality of the samples was evaluated (Kolmogorov-Smirnov test) and Mann–Whitney test (for non-normal distribution) was used. (G) $[Ca^{2+}]_{OMM}$ steady state (basal) and peak measurements upon ATP, CPA and OGD treatment protocol with the N33D3cpv sensor.
(TIF)

S1 Raw images.
(PDF)

Acknowledgments

We would like to thank Roger Tsien for the D3cpv construct (University of California, San Diego, CA) and Marta Giacomelo, Paola Pizzo and Tullio Pozzan for the N33D1cpv construct (Department of Biomedical Sciences, University of Padova, Italy). HeLa WT and TKO IP3Rs cells were a gift from Katsuhiko Mikoshiba, SIAIS, ShanghaiTech University, Shanghai, China. We address a special thanks to Mélanie Paillard and Mariam Wehbi for proofreading the manuscript.

Author Contributions

Conceptualization: Yves Gouriou, Fabrice Gonnot, Gabriel Bidaux.

Data curation: Yves Gouriou, Fabrice Gonnot.

Formal analysis: Yves Gouriou, Fabrice Gonnot.

Funding acquisition: Ludovic Gomez, Gabriel Bidaux.

Investigation: Yves Gouriou, Fabrice Gonnot, Mariam Wehbi, Camille Brun.

Methodology: Yves Gouriou, Fabrice Gonnot.

Supervision: Gabriel Bidaux.

Writing – original draft: Yves Gouriou.

Writing – review & editing: Yves Gouriou, Ludovic Gomez, Gabriel Bidaux.

References

1. Schlaepfer WW, Bunge RP. Effects of calcium ion concentration on the degeneration of amputated axons in tissue culture. The Journal of cell biology. 1973;59(2 Pt 1):456–70. https://doi.org/10.1083/jcb.59.2.456 PMID: 4805010; PubMed Central PMCID: PMC2109098.
2. Schanne FA, Kane AB, Young EE, Farber JL. Calcium dependence of toxic cell death: a final common pathway. Science. 1979; 206(4419):700–2. https://doi.org/10.1126/science.386513 PMID: 386513
3. Paschen W, Doutheil J. Disturbances of the functioning of endoplasmic reticulum: a key mechanism underlying neuronal cell injury? Journal of cerebral blood flow and metabolism: official journal of the International Society of Cerebral Blood Flow and Metabolism. 1999; 19(1):1–18. https://doi.org/10.1097/00004647-199901000-00001 PMID: 9886350.
4. Lemos FO, Bultynck G, Parys JB. A comprehensive overview of the complex world of the endo- and sarcoplasmic reticulum Ca(2+)-leak channels. Biochimica et biophysica acta Molecular cell research. 2021; 1868(7):119020. https://doi.org/10.1016/j.bbamcr.2021.119020 PMID: 33798602.
5. Szabadkai G, Bianchi K, Varnai P, De Stefani D, Wieckowski MR, Cavagna D, et al. Chaperone-mediated coupling of endoplasmic reticulum and mitochondrial Ca2+ channels. The Journal of cell biology. 2006; 175(6):901–11. https://doi.org/10.1083/jcb.200608073 PMID: 17178908; PubMed Central PMCID: PMC2064700.
6. Gomez L, Thiebaut PA, Paillard M, Ducreux S, Abrial M, Crola Da Silva C, et al. The SR/ER-mitochondria calcium crosstalk is regulated by GSK3beta during reperfusion injury. Cell death and differentiation. 2016; 23(2):313–22. Epub 2015/07/25. https://doi.org/10.1038/cdd.2015.101 PMID: 26206086; PubMed Central PMCID: PMC4716295.
7. Paillard M, Tubbs E, Thiebaut PA, Gomez L, Fauconnier J, Da Silva CC, et al. Depressing mitochondria-reticulum interactions protects cardiomyocytes from lethal hypoxia-reoxygenation injury. Circulation. 2013; 128(14):1555–65. Epub 2013/08/29. https://doi.org/10.1161/CIRCULATIONAHA.113.001225 PMID: 23983249.
8. Lu F, Tian Z, Zhang W, Zhao Y, Bai S, Ren H, et al. Calcium-sensing receptors induce apoptosis in rat cardiomyocytes via the endo(sarco) plasmic reticulum pathway during hypoxia/reoxygenation. Basic & clinical pharmacology & toxicology. 2010; 106(5):396–405. https://doi.org/10.1111/j.1742-7843.2009.00502.x PMID: 20030631.
9. Paquot F, Huart J, Defraigne JO, Krzesinski JM, Jouret F. Implications of the calcium-sensing receptor in ischemia/reperfusion. Acta cardiologica. 2017; 72(2):125–31. https://doi.org/10.1080/00015385.2017.1291136 PMID: 28597792.
10. Yan L, Zhu T, Sun T, Wang L, Pan S, Tao Z, et al. Activation of calcium-sensing receptors is associated with apoptosis in a model of simulated cardiomyocytes ischemia/reperfusion. Journal of biomedical research. 2010; 24(4):301–7. https://doi.org/10.1016/S1674-8301(10)60042-5 PMID: 23554644; PubMed Central PMCID: PMC3596596.
11. Bruno V, Battaglia G, Copani A, D'Onofrio M, Di Iorio P, De Blasi A, et al. Metabotropic glutamate receptor subtypes as targets for neuroprotective drugs. Journal of cerebral blood flow and metabolism: official journal of the International Society of Cerebral Blood Flow and Metabolism. 2001; 21(9):1013–33. https://doi.org/10.1097/00004647-200109000-00001 PMID: 11524608.
12. Szydlowska K, Tymianski M. Calcium, ischemia and excitotoxicity. Cell calcium. 2010; 47(2):122–9. https://doi.org/10.1016/j.ceca.2010.01.003 PMID: 20167368.
13. Tsien RY. The green fluorescent protein. Annual review of biochemistry. 1998; 67:509–44. https://doi.org/10.1146/annurev.biochem.67.1.509 PMID: 9759496.
14. Palmer AE, Giacomello M, Kortemme T, Hires SA, Lev-Ram V, Baker D, et al. Ca2+ indicators based on computationally redesigned calmodulin-peptide pairs. Chemistry & biology. 2006; 13(5):521–30. https://doi.org/10.1016/j.chembiol.2006.03.007 PMID: 16720273.
15. Giacomello M, Drago I, Bortolozzi M, Scorzeto M, Gianelle A, Pizzo P, et al. Ca2+ hot spots on the mitochondrial surface are generated by Ca2+ mobilization from stores, but not by activation of store-

operated Ca2+ channels. Molecular cell. 2010; 38(2):280–90. https://doi.org/10.1016/j.molcel.2010.04.003 PMID: 20417605.

16. Giacomello M, Pellegrini L. The coming of age of the mitochondria-ER contact: a matter of thickness. Cell death and differentiation. 2016; 23(9):1417–27. Epub 2016/06/25. https://doi.org/10.1038/cdd.2016.52 PMID: 27341186; PubMed Central PMCID: PMC5072433.

17. Palmer AE, Tsien RY. Measuring calcium signaling using genetically targetable fluorescent indicators. Nature protocols. 2006; 1(3):1057–65. https://doi.org/10.1038/nprot.2006.172 PMID: 17406387.

18. Gouriou Y, Bijlenga P, Demaurex N. Mitochondrial Ca2+ uptake from plasma membrane Cav3.2 protein channels contributes to ischemic toxicity in PC12 cells. J Biol Chem. 2013; 288(18):12459–68. Epub 2013/03/20. https://doi.org/10.1074/jbc.M112.428128 PMID: 23508951; PubMed Central PMCID: PMC3642294.

19. Gouriou Y, Alam MR, Harhous Z, Crola Da Silva C, Baetz DB, Badawi S, et al. ANT2-Mediated ATP Import into Mitochondria Protects against Hypoxia Lethal Injury. Cells. 2020;9(12). https://doi.org/10.3390/cells9122542 PMID: 33255741; PubMed Central PMCID: PMC7760820.

20. Ando H, Hirose M, Mikoshiba K. Aberrant IP3 receptor activities revealed by comprehensive analysis of pathological mutations causing spinocerebellar ataxia 29. Proceedings of the National Academy of Sciences of the United States of America. 2018; 115(48):12259–64. https://doi.org/10.1073/pnas.1811129115 PMID: 30429331; PubMed Central PMCID: PMC6275503.

21. Yue L, Wang L, Du Y, Zhang W, Hamada K, Matsumoto Y, et al. Type 3 Inositol 1,4,5-Trisphosphate Receptor is a Crucial Regulator of Calcium Dynamics Mediated by Endoplasmic Reticulum in HEK Cells. Cells. 2020;9(2). https://doi.org/10.3390/cells9020275 PMID: 31979185; PubMed Central PMCID: PMC7072192.

22. Bandara S, Malmersjo S, Meyer T. Regulators of calcium homeostasis identified by inference of kinetic model parameters from live single cells perturbed by siRNA. Science signaling. 2013;6(283):ra56. https://doi.org/10.1126/scisignal.2003649 PMID: 23838183; PubMed Central PMCID: PMC3897207.

23. Kasri NN, Kocks SL, Verbert L, Hebert SS, Callewaert G, Parys JB, et al. Up-regulation of inositol 1,4,5-trisphosphate receptor type 1 is responsible for a decreased endoplasmic-reticulum Ca2+ content in presenilin double knock-out cells. Cell calcium. 2006; 40(1):41–51. https://doi.org/10.1016/j.ceca.2006.03.005 PMID: 16675011.

24. Bartok A, Weaver D, Golenar T, Nichtova Z, Katona M, Bansaghi S, et al. IP3 receptor isoforms differently regulate ER-mitochondrial contacts and local calcium transfer. Nature communications. 2019; 10(1):3726. https://doi.org/10.1038/s41467-019-11646-3 PMID: 31427578; PubMed Central PMCID: PMC6700175.

25. Berridge MJ. Inositol trisphosphate and diacylglycerol: two interacting second messengers. Annual review of biochemistry. 1987; 56:159–93. https://doi.org/10.1146/annurev.bi.56.070187.001111 PMID: 3304132.

26. Tateishi Y, Hattori M, Nakayama T, Iwai M, Bannai H, Nakamura T, et al. Cluster formation of inositol 1,4,5-trisphosphate receptor requires its transition to open state. J Biol Chem. 2005; 280(8):6816–22. Epub 2004/12/08. https://doi.org/10.1074/jbc.M405469200 PMID: 15583010.

27. Pinton P, Pozzan T, Rizzuto R. The Golgi apparatus is an inositol 1,4,5-trisphosphate-sensitive Ca2+ store, with functional properties distinct from those of the endoplasmic reticulum. EMBO J. 1998; 17(18):5298–308. Epub 1998/09/16. https://doi.org/10.1093/emboj/17.18.5298 PMID: 9736609; PubMed Central PMCID: PMC1170857.

28. Quesada I, Chin WC, Steed J, Campos-Bedolla P, Verdugo P. Mouse mast cell secretory granules can function as intracellular ionic oscillators. Biophys J. 2001; 80(5):2133–9. Epub 2001/04/28. https://doi.org/10.1016/S0006-3495(01)76186-3 PMID: 11325716; PubMed Central PMCID: PMC1301405.

29. Mitchell KJ, Pinton P, Varadi A, Tacchetti C, Ainscow EK, Pozzan T, et al. Dense core secretory vesicles revealed as a dynamic Ca(2+) store in neuroendocrine cells with a vesicle-associated membrane protein aequorin chimaera. The Journal of cell biology. 2001; 155(1):41–51. Epub 2001/09/26. https://doi.org/10.1083/jcb.200103145 PMID: 11571310; PubMed Central PMCID: PMC2150797.